ACS APPLIED MATERIALS & INTERFACES

Research Article

www.acsami.org

Nanostructured Biointerfacing of Metals with Carbon Nanotube/Chitosan Hybrids by Electrodeposition for Cell Stimulation and Therapeutics Delivery

Kapil D. Patel,[†,‡] Tae-Hyun Kim,[†,‡] Eun-Jung Lee,[†,‡] Cheol-Min Han,[†,§] Ja-Yeon Lee,[†,‡] Rajendra K. Singh,[†,‡] and Hae-Won Kim*[,†,‡,§]

[†]Institute of Tissue Regeneration Engineering (ITREN), [‡]Department of Nanobiomedical Science & BK21 PLUS NBM Global Research Center for Regenerative Medicine, and [§]Department of Biomaterials Science, College of Dentistry, Dankook University, Cheonan 330-714, South Korea

Supporting Information

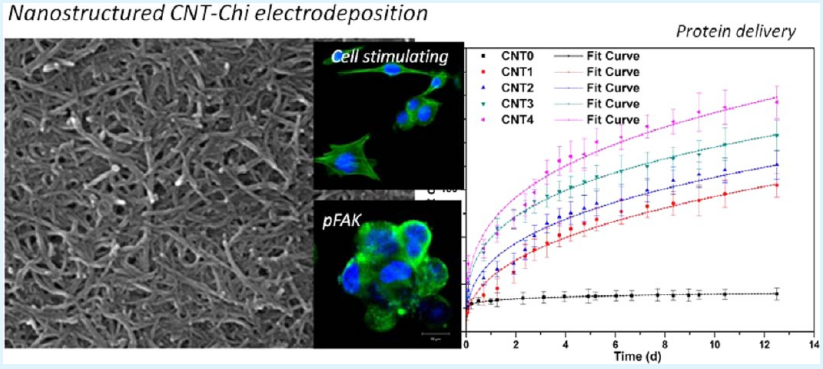

ABSTRACT: Exploring the biological interfaces of metallic implants has been an important issue in achieving biofunctional success. Here we develop a biointerface with nanotopological features and bioactive composition, comprising a carbon nanotube (CNT) and chitosan (Chi) hybrid, via an electrophoretic deposition (EPD). The physicochemical properties, in vitro biocompatibility, and protein delivering capacity of the decorated nanohybrid layer were investigated, to address its potential usefulness as bone regenerating implants. Over a wide compositional range, the nanostructured hybrid interfaces were successfully formed with varying thicknesses, depending on the electrodeposition parameters. CNT-Chi hybrid interfaces showed a time-sequenced degradation in saline water, and a rapid induction of hydroxyapatite mineral in a simulated body fluid. The nanostructured hybrid substrates stimulated the initial adhesion events of the osteoblastic cells, including cell adhesion rate, spreading behaviors, and expression of adhesive proteins. The nanostructured hybrid interfaces significantly improved the adsorption of protein molecules, which was enabled by the surface charge interaction, and increased surface area of the nanotopology. Furthermore, the incorporated protein was released at a highly sustained rate, profiling a diffusion-controlled pattern over a couple of weeks, suggesting the possible usefulness as a protein delivery device. Collectively, the nanostructured hybrid CNT-Chi layer, implemented by an electrodeposition, is considered a biocompatible, cell-stimulating, and protein-delivering biointerface of metallic implants.

KEYWORDS: *nanostructured surface, carbon nanotubes, coatings, electrodeposition, metallic implants, cell adhesion, protein delivery*

1. INTRODUCTION

Metallic materials have been used for hard tissue implants, primarily due to their excellent mechanical properties. Among those, titanium (Ti) and its alloys are most widely used, because of their biocompatibility and corrosion resistance, resulting from a naturally formed passive oxide layer.[1−3] The biocompatibility of Ti and its alloys has a close relationship with their surface properties, such as surface roughness, topography, and chemical composition. In the biomedical field, the materials with nanotopological surface have a lot of merit. It is well-known that the nanotopological feature on the materials surface is one of the most important factors that affect cellular behaviors, such as cell anchorage, migration, proliferation, differentiation, and death.[4−6] Although the cells have micrometer dimensions, they evolve in vivo in close contact with the extracellular matrix (ECM), a matrix with topographical features of nanometer size, made of nanofibers of proteins, such as collagen and elastin, which provide biological and physical support for cell behaviors.[7] Moreover, large surface area is another merit of the nanotopological surface, because it

Received: August 26, 2014
Accepted: October 17, 2014
Published: October 17, 2014

can allow for the surface to deliver a large amount of therapeutic molecules, such as growth factors, by providing numerous attachment sites. Thus, engineering the material surfaces with nanotopological features is currently one of the challenging issues in hard tissue implant fields.

Coating the Ti surface with bioactive materials is one of the simplest and most promising methods of surface modification, which controls surface structure and chemical composition. A lot of effort has been made to coat the Ti surface, by using a range of techniques, such as plasma spraying,[8] anodic oxidation,[9] sol−gel methods,[10] biomimetic coating,[11] microarc oxidation,[12] and electrochemical treatment.[13] The electrophoretic deposition (EPD) is a versatile coating method, which can produce a uniform coating layer, via motion of charged particles toward anode or cathode, under an electric field. The simplicity of process, wide range of coating materials, ease of control of the composition and thickness, applicability to complex shapes, and low cost are advantages of the EPD method. Using the EPD method, Ti has been tailored with various compositions, including bioactive inorganics,[14−16] biodegradable polymers,[17,18] and composites,[19−23] in an attempt to improve the biocompatibility. Furthermore, drug molecules have also been incorporated within the EPD coatings, to improve the therapeutic potential of the coated implants.[20−22]

Here, we focused on bioactive inorganic material and biopolymer composites as a coating material. A considerable effort has been made to produce an inorganic−organic composite coating layer by the EPD process.[19−23] Generally, hydroxyapatite (HA), silica, and their combination, and carbon nanotubes (CNTs) have been used as the inorganic substance. Among these, CNTs were chosen, due to their unique structural merits. The EPD processed CNTs have been shown to have nanoscale fibrous structures, providing Ti substrates with nanotopological surfaces.[22,23] In fact, CNTs have been used not only for coatings, but also for many other applications in the biomedical fields, because of their unique structure, and excellent mechanical and electrical properties despite their potential cytotoxicity.[24−28]

As an organic source of EPD process, chitosan (Chi) has been widely used, because it is biocompatible, biodegradable, and highly charged.[17,19,29] Chi, a natural biopolymer, is obtained by deacetylation of chitin, which is the main component of the exoskeleton of insects, crustaceans, and fungi. Chi is readily soluble, and positively charged in dilute acidic solutions, due to its amine groups.[30] Because of its positively charged property, Chi is easily deposited onto cathode, under an electric field. In order to deposit the CNTs with Chi by the EPD process, CNTs have to be dispersible and stable in an acidic aqueous solution, where Chi is readily soluble. However, pristine CNTs are not soluble in an acidic solution, due to the aggregation caused by hydrophobic interaction, and van der Waals attraction between the nanotubes. Therefore, CNTs were treated in a concentrated nitric acid and sulfuric acid solution, to generate carboxylic acid and hydroxyl groups on the CNT surface, which make CNTs hydrophilic and dispersible in an aqueous solution.[31,32] Moreover, acid-treated CNTs can be well adsorbed onto positively charged Chi, due to the anionic functional groups.[28]

In this study, we aimed to develop a bioactive CNT-Chi composite coating system with nanoscale topographical features through the EPD technique, for improving the biocompatibility of Ti. Pure Chi and Chi composite suspension with various CNT contents were prepared, and then coated onto the Ti surface. The nanotopography, composition, and phase of the coating layer, after the EPD process, were investigated. The physicochemical and biological properties of the coating layers were evaluated, in terms of degradation, mineralization, and osteoblastic cell responses, particularly in the initial adhesion events, such as cell anchorage, involvement of adhesive molecules, and cell spreading. Furthermore, the protein loading and delivery capacity of the coating layer were examined, using bovine serum albumin (BSA) as a model protein, which is considered to be one of the advantages of the nanotopological surface of a CNT-Chi coating layer.

2. MATERIALS AND METHODS

2.1. Acid Treatment of CNTs. In order to improve the dispersibility of CNT in aqueous solution, its surface was modified by acid treatment. The 2 g of multiwalled carbon nanotubes (EM-Power Co., Ltd. Korea) was added into 50 mL of H_2SO_4 (90%, Reagent Duksan, Korea) and 50 mL of HNO_3 (70%, Sigma-Aldrich, USA) mixture solution in two-neck round-bottom flask, and kept at 80 °C for 4 days, under constant magnetic stirring for reflux. The other neck was closed with rubber cap having a thermometer, to record the temperature. After 4 days of continuous reflux, acid treated CNTs were vacuum-filtered through a 0.2 μm mixed cellulose ester membrane, and thoroughly rinsed with deionized water, until the pH of the falling filtrate became neutral. Finally, it was dried under vacuum at 50 °C for 24 h. After surface modification, the dispersibility of CNT increased significantly, and the ζ-potential in distilled water at room temperature decreased, from −4.5 mV to −32.1 mV.

2.2. Preparation of CNT-Chi Suspension and Ti Substrates. Chi (85% deacetylated, Mw = 200 000 Da, Sigma-Aldrich, USA) was dissolved in 1% acetic acid solution, at various concentrations (0.125, 0.25, 0.375, 0.5, and 1 mg/mL).The acetic acid solution was prepared, by adding 1% of acetic acid (Sigma-Aldrich, USA) into an ethanol−water cosolvent (25% of ethanol in water). It is well-known that ethanol plays an important role in reducing the bubble generation, during the EPD process.[33] In a separate preparation, acid treated CNTs were added in ethanol−water cosolvent at 0.5 mg/mL concentration, and acetic acid was slowly added, until the pH was about 3.5. Then, the homogeneously dispersed suspension was obtained, by ultrasonication in ice-cooled water bath. The Chi solutions (0.125−0.5 mg/mL) were mixed with CNT solution drop-by-drop, with a volume ratio of 1:1, while stirring for 2 h. The designations of CNT-Chi composite solutions used in this study are summarized in Supporting Information Table S1. Ti plate (commercially pure grade, Senulbio Biotech, Korea), with a dimension of 10 mm × 10 mm × 1 mm, was prepared as a substrate. The Ti plate was polished with SiC abrasive paper, and cleaned ultrasonically in acetone, ethanol, and distilled water, successively, for 15 min.

2.3. Coating of CNT-Chi Layer by EPD Process. The CNT-Chi composites were coated onto Ti substrate, using the EPD process. Because the ζ-potential of each suspension showed positive value, CNT-Chi composites were coated onto Ti, via cathodic EPD process. The Ti and stainless steel plates were placed on cathode and anode, respectively, and the distance between cathode and anode was 11 mm. After degassing by ultrasonication, the EPD process was carried out in each suspension, under the DC fields (N5771A, 300 V/5A;

Agilent Technologies). The weight change of samples, due to the EPD process, with various applied voltages and deposition times, was measured. For further tests, CNT-Chi coating layers with the same thickness were obtained, under an applied voltage of 15 V for 3 min. The coating compositions are summarized in Supporting Information Table S1. During the EPD process, the pH of each suspension was maintained at between 3.4 and 3.6, to obtain a uniform coating layer. After the coating process, specimens were taken, washed gently with ethanol and distilled water, and dried, for further characterizations and evaluations.

2.4. Characterizations of Coating Layers. The topography of coating surfaces and cross-sectional images was assessed by field emission scanning electron microscopy (FE-SEM; Tescan Mira II LMH, Czech Republic). The quantity of CNTs in the coating layer was deduced by thermogravimetric analysis (TGA; TGA N-1500, Scinco, Korea). TGA analysis was carried out, using a portion of coating layer scraped from the substrate at temperature up to 800 °C, at a heating rate of 10 °C min^{-1} in N_2 gas. The chemical bonds and the phase of the coating layer were investigated by attenuated total reflection Fourier transformation infrared spectroscopy (ATR-FTIR; Varian 640-IR, Varian, Australia), and X-ray diffraction (XRD; Ultima IV, Ringku, Japan), respectively.

The degradability of the coating layer was studied in phosphate buffered saline (PBS; Sigma, USA) solution. Each specimen was immersed in 15 mL of PBS solution, and incubated at 37 °C. The specimen was taken out at predetermined periods (3, 7, 14, 21, 28 days), dried, and the weight change was recorded. The apatite forming ability of the CNT-Chi coating layer was studied in a modified simulated body fluid, whose ionic concentration was twice the normal simulated body fluid (2 × SBF; Na^+, K^+, Mg^{2+}, Ca^{2+}, Cl^-, HCO_3^-, HPO_4^{2-}, and SO_4^{2-} were 284.0, 10.0, 3.0, 5.0, 295.6, 8.4, 2.0, and 1.0, respectively). Each specimen was immersed in 10 mL of 2 × SBF solution, and incubated at 37 °C, for various periods (3, 7, 10, 14, 21, 28 days). At each time, the specimen was taken out, rinsed with distilled water, and dried. The changes in surface morphology and weight due to apatite formation were observed by FE-SEM, and recorded, respectively. For both degradability and apatite forming ability tests, 3 replicate specimens were used, and averaged.

2.5. Cell Assays on Coating Layers. The in vitro biological properties of the CNT-Chi composite coatings were addressed, by means of initial cell adhesion behaviors, including attached cell number and cell spreading degree. Furthermore, the expression of adhesive proteins was assessed, by means of immuno-cytochemistry. Prior to cell seeding, all samples were sterilized, by immersion in 70% ethanol for 30 min, and exposure to UV irradiation, overnight. The preincubated MC3T3-E1 cells (osteoblastic cell line, ATCC, USA) were placed onto the sterilized specimens, at the densities of either 2×10^4 or 5×10^4. The cells were then cultured in α-minimal essential medium (α-MEM; Thermo Scientific HyClone, South Logan, UT), supplemented with 10% fetal bovine serum (FBS; Gibco, USA) and 1% penicillin–streptomycin (Invitrogen, USA), under 5% CO_2/95% air, at 37 °C.

The cell anchorage and spreading behaviors were assessed, by fluorescent microscopy observation. After 6 and 18 h of culturing, the cells were fixed with 4% paraformaldehyde solution, washed in PBS, permeabilized with 0.1% Triton X-100 solution, and washed in PBS again. After blocking the nonspecific sites with 1% BSA solution, F-actin and nuclei were stained with phalloidin and 4′,6-diamidino-2-phenylindole (DAPI), respectively. A number of the stained cell morphologies (4–5 field images for each group) were obtained by the fluorescent microscopy (IX7151Olympus, Japan). Based on the cell images, the cell spreading was evaluated, by measuring the length of cellular extensions. The cells were classified into two groups by their aspect ratio—the ratio between the length (l) of cell (most elongated direction), and the width (d) of the cell (the shortest direction); round cells ($d/l < 1.5$), and spread cells ($d/l > 1.5$). Furthermore, the length of the cellular extensions was compared.

Cells positive for the expression of adhesion proteins, including focal adhesion kinase (FAK), paxillin, and vinculin, were immunofluorescence-stained. Cells cultured for 4 h on each substrate were fixed in ice-cold 4% paraformaldehyde solution and then stained with each primary antibody included anti-FAK (phospho Y576; pFAK, abcam, USA), anti-paxillin (phospho Y181; pPaxillin, abcam), and anti-vinculin (abcam) for 12 h at 4 °C. The stained cells were then incubated with FITC-conjugated secondary antibodies (Santa Cruz, USA). The cells were counterstained with DAPI to observe the nuclear morphology. Fluorescent images were observed under a LSM 700 laser-scanning confocal microscope.

2.6. Protein Adsorption and Release Tests. BSA (Sigma-Aldrich, USA) was used as a model protein for the adsorption and release tests. In order to find the BSA adsorption capacity of the CNT-Chi coating layer, the adsorption isotherm was studied. Coating samples were immersed in 1 mL of BSA solution in PBS, prepared with various concentrations (0.2–5 mg/mL). After incubation at 37 °C for 12 h, the samples were taken out, and the BSA concentrations of the solution were assessed, by measuring the absorbance at 278 nm, using UV–visible spectrophotometer (Libra S22, Biochrom, UK). The amount of BSA adsorbed onto the sample surface was calculated, by subtracting the final amount from the initial amount.

The release behavior the BSA from the coatings was also examined. The BSA loading carried out in 2 mg/mL concentration was used for the release study. The samples were then soaked into PBS, and kept statically at 37 °C for different times. At each time point, the whole medium was replaced with fresh PBS, and the BSA concentration of the withdrawn medium was assessed using UV–visible spectrophotometer.

2.7. Statistical Analysis. Data were analyzed by the Student's t-test. All data are presented as the mean ± 1 standard deviation (SD), and statistical significance was considered at $p < 0.05$.

3. RESULTS AND DISCUSSION

3.1. CNTs and EPD Process. EPD is a versatile technique for the surface modification of metallic materials. The EPD process involves the movements of charged particles in a suspension. Therefore, characterization of the raw materials and suspension is very important. Figure 1 shows the characteristics of the CNTs prepared for the EPD coating. A typical TEM morphology of multiwalled CNTs shows the nanosized structure of CNTs, with a diameter of 25 nm, and a wall thickness of 5 nm (Figure 1a). The surface of CNTs was functionalized via acid treatment, to enhance dispersion ability in aqueous solution. While the FTIR spectrum of the as-received CNTs displayed two peaks, related to C═C and O—

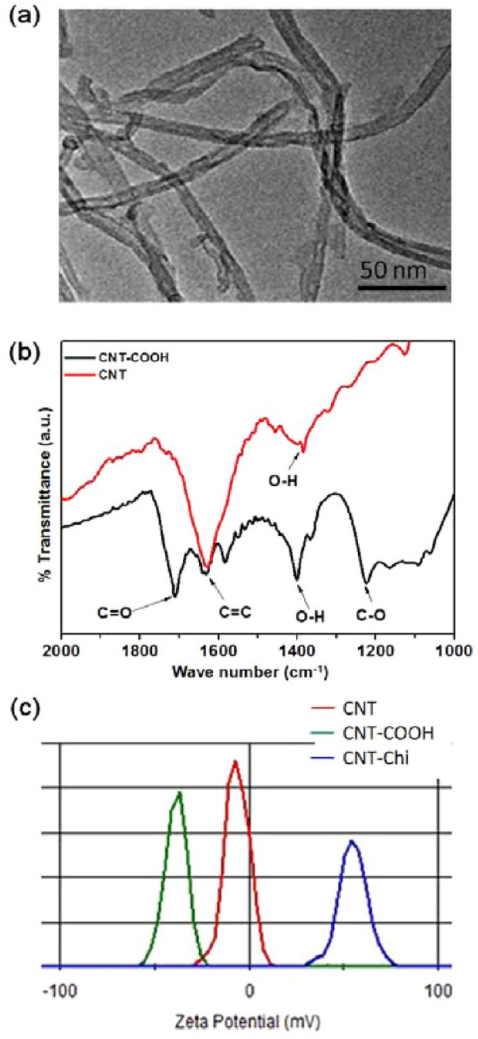

Figure 1. Characteristics of CNTs: (a) TEM images of multiwalled CNTs after carboxylation; (b) FT-IR spectra of CNTs before and after carboxylation, signifying the development of surface functional groups (C═O and C—O) by strong acid treatment; (c) ζ-potential of native CNTs, carboxylated CNT and CNT-Chi solution in distilled water, showing a dramatic change in the surface charge properties of the CNTs, from −4.5 mV (native) to −38.5 mV (carboxylated), and oppositely to +48.2 mV (complexed with Chi).

H bonds at 1635 and 1400 cm^{-1},[34,35] two additional peaks related to −COOH functional group, such as C═O and C—O bonds at 1710 and 1225 cm^{-1},[36] and C═C stretching associated with backbone structure at 1585 cm^{-1}[37] appeared, after acid treatment (Figure 1b). The increment of peak intensity of the O—H bond is additional evidence of the formation of −COOH functional groups. The ζ-potential of the CNTs dispersed in distilled water changed from slightly negative (−4.5 mV), to highly negative (−38.5 mV) after acid treatment, confirming the successful carboxylic acid functionalization of the surface. Furthermore, the ζ-potential of acid-treated CNTs changed to highly positive (+48.2 mV), after mixing with Chit solution, which reflects the nature of positively-charged Chit molecules (Figure 1c). This result suggests that CNT-Chi suspension can be used for cathodic EPD process. During EPD in an acidic solution, Chi molecules become positively charged; therefore, negatively charged CNTs easily react with Chi matrix. After reaction, the CNT-Chi hybrid is still positively charged. Thus, CNT-Chi was deposited onto Ti substrate by electrophoresis, when negative potential was applied.[33,38]

3.2. Characteristics of CNT-Chi Hybrid Coatings. The properties of a coating layer can be easily controlled, by adjusting the EPD parameters, including pH of suspension, applied voltage and deposition time. In a previous study, the homogeneity and uniformity of the Chi-based coating layer could be achieved, when the pH of suspension was between 3.1 and 3.6.[20] In this study, therefore, the pH of the CNT-Chi solution was fixed at 3.45. During the electrodeposition process, the weight gain of the coating by varying the applied voltage and deposition time was observed, as shown in Figure 2. At first, the electrodeposition process was carried out at various applied voltages, with a fixed deposition time of 3 min. A linear increment of weight gain with voltage change from 10 to 40 V was found (Figure 2a). At a fixed applied voltage of 15 V, the weight gain as a function of time was also almost linear (Figure 2b). With regard to the effects of composition on the coating weight gain, although the exact relationship could not be drawn, the incorporation of CNTs appeared to slightly decrease the coating weight gain. In fact, Chi molecules have already proven excellent mobility in the EPD cathodic coating, due to the highly positively charged surface. Although the Chi molecules would decorate the surface of negatively charged CNTs, the mobility for cathodic deposition is considered to decrease, compared to the case for native Chi. Compared to the CNT1,

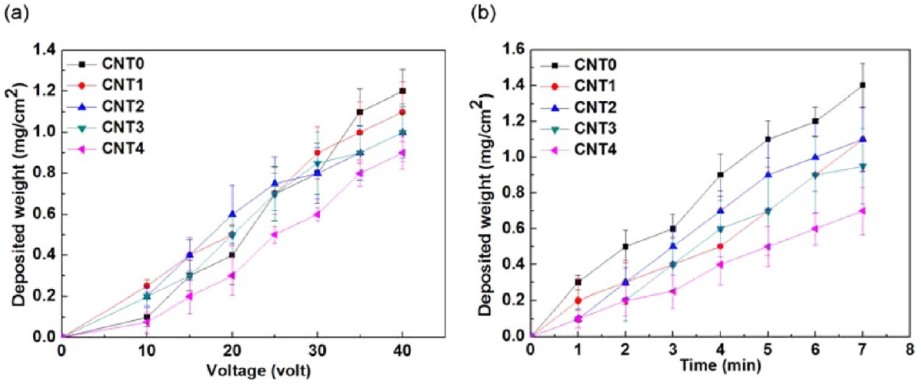

Figure 2. Weight gain during the EPD coating, measured with varying the coating parameters, applied voltage and time, at pH = 3.45 of suspensions: (a) for fixed deposition time of 3 min, as a function of applied voltage, and (b) for fixed applied voltage at 15 V, as a function of time.

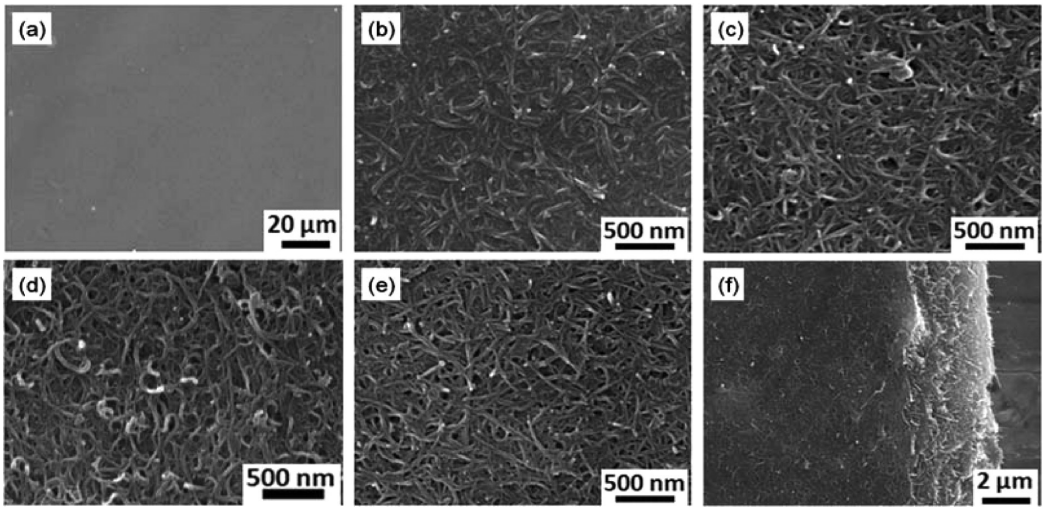

Figure 3. SEM images of the surface morphologies of the coating layers: (a) CNT0, (b) CNT1, (c) CNT2, (d) CNT3, and (e) CNT4. In (f), the cross-sectional SEM images of the CNT3 on Ti substrate reveal the coating layer. All coatings were performed at 15 V for 3 min, at pH 3.45.

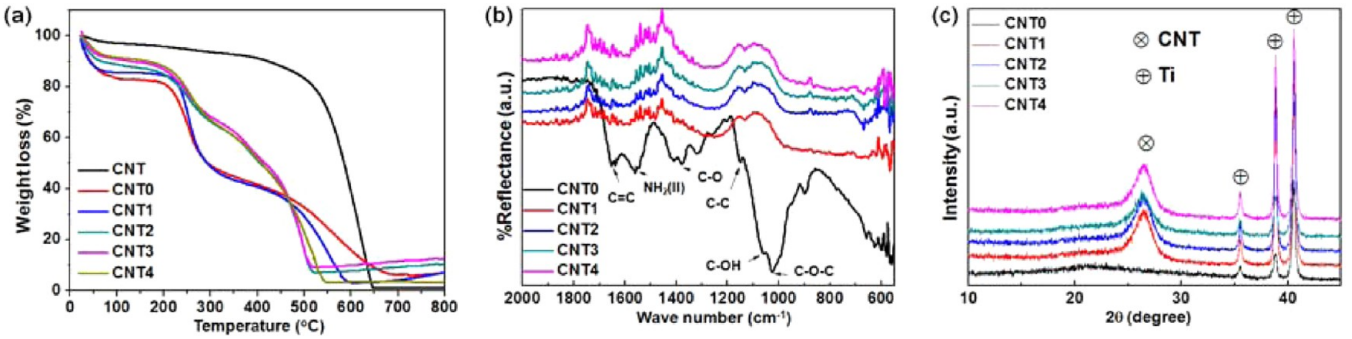

Figure 4. Characterization of the hybrid coatings. (a) Thermogravimetric analyses measured up to 800 °C, (b) FT-IR spectra, and (c) XRD patterns.

CNT2, and CNT3, CNT4 appeared to show more substantial decrease in the coating weight gain, which can be explained as follows: below certain concentration of CNTs, the surface decoration of Chi molecules is considered to be effective; and above the concentration, excess surface of CNTs would exist, and the limit composition herein is considered to be CNT3. While the coatings showed a slight difference in the weight gain, all the coating compositions produced herein stably adhered to the Ti substrate, not allowing the ease of scratching, peeling off, and delaminating, even after ultrasonic vibration in water. This was presumably because of the relatively thin (5 ± 2 μm) coating thickness achieved and the possible strong bonds between CNT and Chi molecules.

The representative high resolution electron morphologies of CNT-Chi coatings on Ti are shown in Figure 3. CNT0, a pure chitosan coating, showed a dense and homogeneous film (Figure 3a). In contrast to the smooth morphology, CNT-Chi hybrid coatings showed significantly different nanoscale morphology (Figure 3b–e). The CNT's nanofibrous morphology was well reflected. The diameter of nanofibers in the SEM image was similar to that of CNTs observed in the TEM image. The amount of Chi played an important role in the different nanoscale morphologies. When the amount of Chi is relatively high (CNT1), the interspacings between CNTs were largely filled with Chi, which makes the surface quite dense, and relatively smooth (Figure 3b). However, as the content of CNTs increased (CNT2 to CNT4, Figure 3c–e), the interspacings between CNTs became open, making the morphology nanoporous and rough. The nanopores formed throughout the coatings were in the range of a few tens to hundreds of nanometers. The thickness of the coating layer was measured from the cross-sectional tilted images. The image of the CNT3 was representatively examined, by scratching off the sample from the Ti (Figure 3f), which revealed a thickness of about 5 μm. The thickness of the other coating layers was observed in a similar range to that of CNT3.

The CNT-Chi hybrid coating layers were further characterized, as shown in Figure 4. The composition of the CNT-Chi coating layer was investigated by TGA (Figure 4a). In the case of pure CNT, two distinct weight losses were observed: first, 20% of weight loss below 400 °C was attributed to the thermal decomposition of carboxylic acid group on the CNT surface, and 80% of weight loss at 600 °C was due to the thermal degradation of CNT. In fact, the TGA result of pure Chi coating layer has shown three distinct weight losses: first, 22% below 200 °C was attributed to the liberation of adsorbed water, and two further weight losses, of 40% at 200–300 °C, and 38% at 300–550 °C, were from the thermal degradation of pure Chi.[20] The CNT-Chi hybrid coating layers showed almost combined thermal degradation, and the behaviors of CNT2, CNT3, and CNT4, compared to those of CNT0 and CNT1, were much closer to that of pure CNT, implying the higher CNT content in the former coatings. The ATR-FTIR spectra of pure Chi and CNT-Chi hybrid coating layers are shown (Figure 4b); bands related to chitosan (897, 1025, 1318, 1375, 1410, 1560, and 1650 cm^{-1}) were clearly observed, in the case of

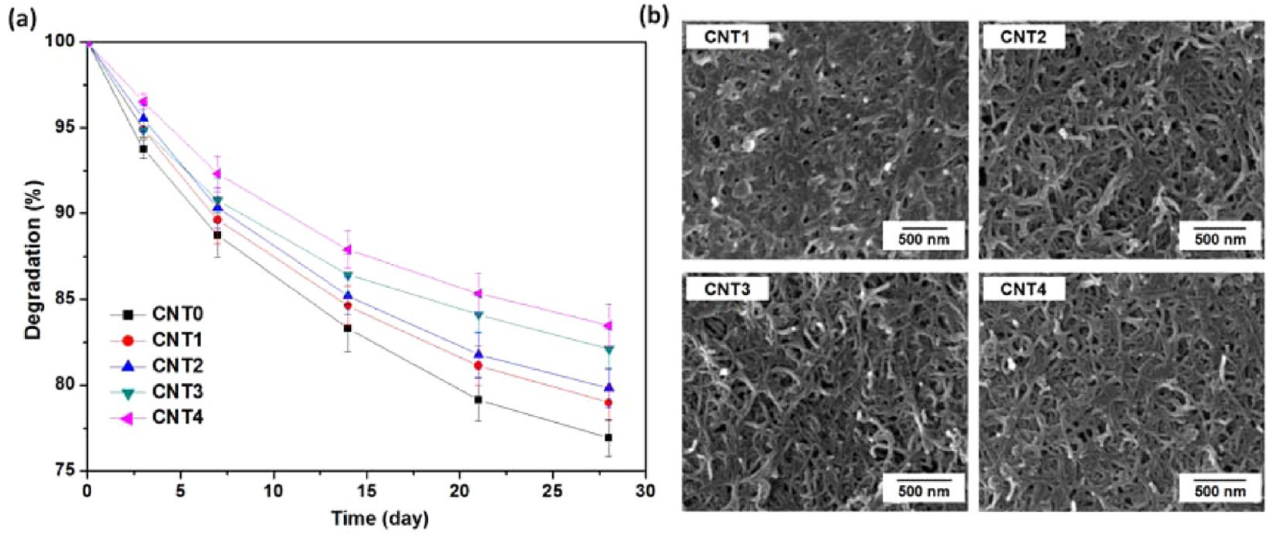

Figure 5. Degradation behavior of the hybrid coatings in PBS, up to 28 days. (a) The weight loss pattern of the coatings (n = 3) with time, and (b) the SEM morphology after 14 days.

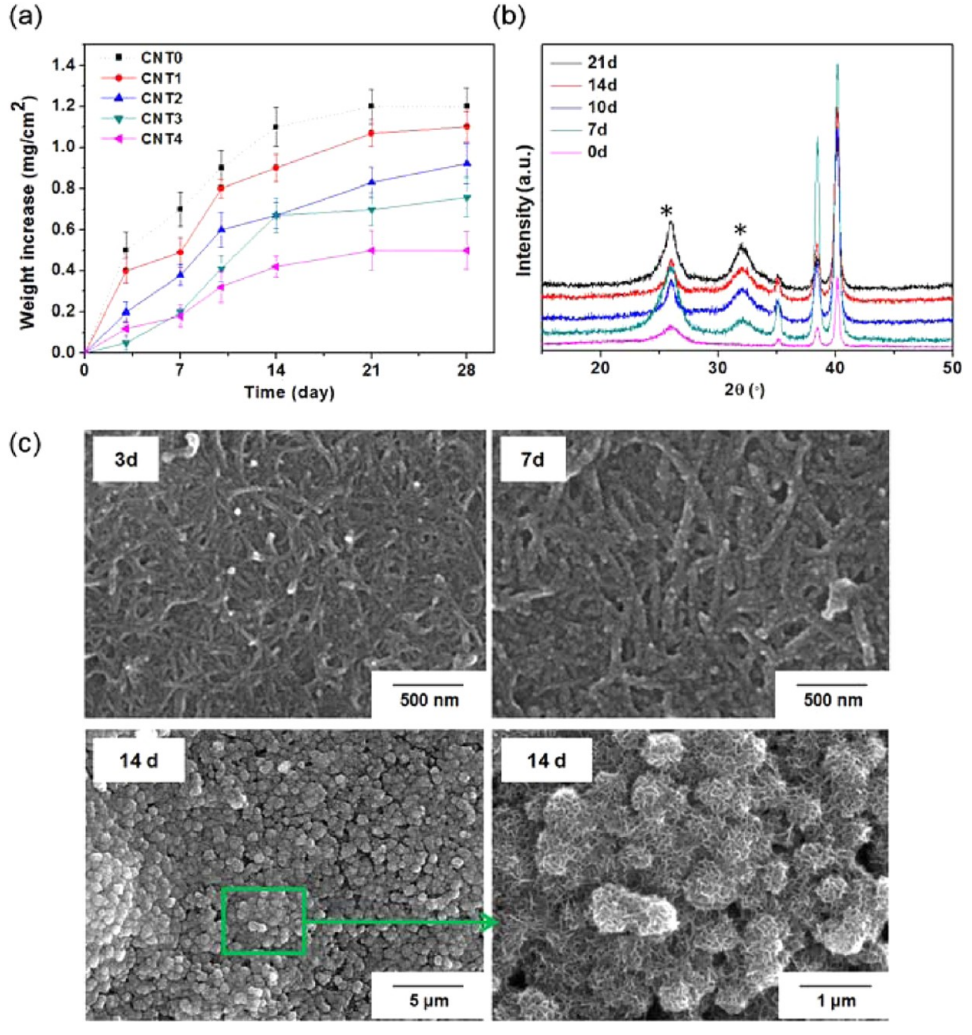

Figure 6. Characterization of the coatings, after incubation in concentrated SBF at 37 °C; (a) weight increase of the coatings, during incubation of the sample for periods of up to 28 days (n = 3), (b) XRD phase analysis, and (c) SEM morphological observation of mineralized surface. The CNT2 specimen was chosen, for representative sample for XRD and SEM analyses.

CNT0.[39] However, in the case of CNT-Chi hybrid coatings, the intensity of peaks related to Chi, such as the amide group, decreased significantly, because of the reduced amount of Chi. The XRD spectra of CNT-Chi hybrid and pure Chi coating

dx.doi.org/10.1021/am505759p | ACS Appl. Mater. Interfaces 2014, 6, 20214−20224

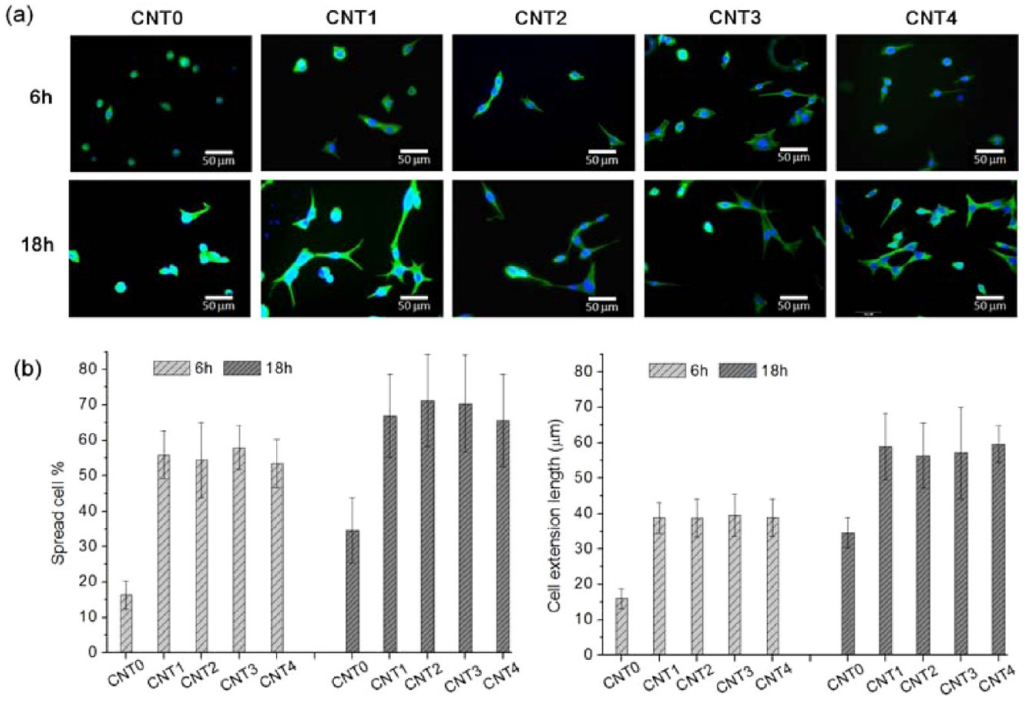

Figure 7. (a) CLSM images of cells initially adhered, and spread onto the nanostructured hybrid coating substrates. Images taken at different time points (6 and 18 h), with costains of F-actins (green) and nuclei (blue). (b) Analyses of the initial cellular behaviors based on the CLSM images, including spreading cell fraction and length of cellular extensions, showed significant difference between CNT0 and CNT-Chi hybrid coatings.

layers are shown (Figure 4c). In the case of pure Chi coating, crystalline phases of Ti substrate at $2\theta \sim 36°$, 39°, and 41° and an amorphous phase of Chi at $2\theta \sim 21°$ were observed. After hybrid coating, a peak at $2\theta \sim 26.2°$ appeared, which is related to CNT.

3.3. In Vitro Degradation and Apatite Forming Ability. The CNT-Chi hybrid coatings were further characterized, in term of in vitro degradation, and apatite forming (mineralization) ability. The degradation behaviors of the coatings were investigated in PBS, as shown in Figure 5. The weight loss of coating layers during the degradation test was monitored, for up to 28 days (Figure 5a). In all cases, the degradation trend was similar, showing a gradual decrease in weight loss with time. The incorporation of CNT decreased the degradation rate. For pure Chi coating layer, the degradation was 7% for 3 days, ~12% for 7 days, ~17% for 14 days, 22% for 21 days, and ~24% for 28 days; while degradation of the CNT4 coating layer was ~3% for 3 days, ~8% for 7 days, ~12% for 14 days, ~14% for 21 days, and ~16% for 28 days. The degradation of the coatings also affected the nanotopography. The SEM images, taken after 14 days of degradation test (Figure 5b), showed more porous surface morphologies than those of the as-deposited surfaces. The morphology of the degraded coatings still showed the nanofibrous morphology of the CNTs. Especially, nanopores were also observed on the CNT1 surface, due to the degradation, which however, have originally shown a dense morphology. Based on this, it is considered that the degradation mainly occurred at the water-soluble chitosan phase.

Along with the degradation behavior in the saline solution, the in vitro apatite forming ability of the coating layers was assessed in simulated body fluid (SBF) solution. Here, we prepared an acceleration medium, 2× SBF, to shorten the investigation period, which has been widely used for the in vitro apatite formation test.[20,40,41] The weight gain of the coatings during immersion of the samples was observed at varying time periods, of up to 28 days (Figure 6a). All the coatings showed weight gain with gradual increase with time, and the degree of weight gain increased, as the amount of Chi increased. This result suggested that Chit played an important role in the apatite formation process. Amino groups of Chi molecules attract phosphate ions in SBF, which subsequently attract calcium ions, resulting in the nucleation and crystallization of apatite.[42] Therefore, the reaction between the amino groups of Chi and carboxylic acid groups of CNT during the EPD process would lower the reactivity of Chi molecules, for the nucleation of apatite. Nevertheless, it should be noted that the CNT-Chi hybrid coatings showed a substantial apatite formation rate. The phase and the morphology of apatite crystals formed on CNT2, a representative sample, were analyzed by XRD and SEM (Figures 6b,c). The main apatite peak at $2\theta \sim 32°$ appeared additionally during the immersion, and became sharper and more apparent, with increasing immersion time. After 3 days of immersion in the SBF, some mineral islands started to grow on the surface of the CNTs; and they were clearly seen on the surface, while preserving the CNT-related nanotopography, at day 7. At day 14, the minerals covered the whole surface, totally changing the nanofibrous morphology, and the mineralized crystal size became significantly enlarged. Based on these results, it is considered that the CNT-Chi hybrid coatings had substantial apatite formation ability, i.e., excellent in vitro bone-bioactivity.

3.4. Effects on Initial Osteoblastic Responses. To demonstrate that the CNT-Chi hybrid coating surface would provide a substrate condition for osteoblastic cellular anchorage and growth, we cultured murine preosteoblastic MC3T3-E1 cells on coatings, for different time points. In particular, initial cellular events at the early time points were investigated. First, cell anchorage and spreading images on each coating sample were taken by fluorescence microscope, at varying time points

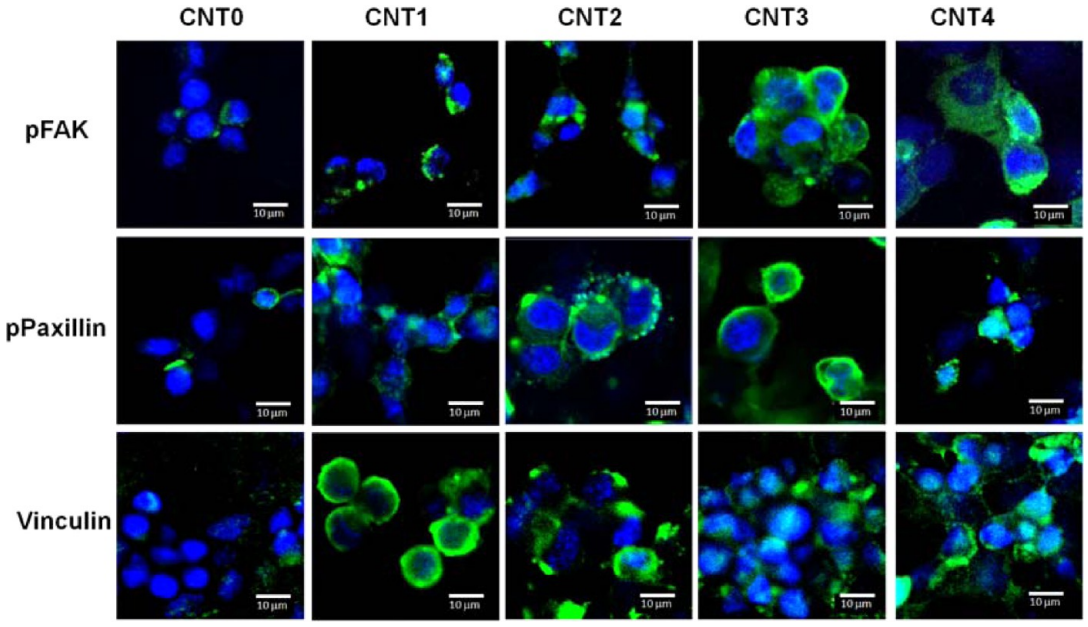

Figure 8. Adhesive molecules possibly involved in the initial cell adhesion events, analyzed by immunostaining images. Signals positive for p-FAK, p-paxillin, and vinculin were strongly expressed in all the CNT-Chi hybrid coatings but not in CNT0.

of 6 and 18 h (Figure 7a). On CNT0 coating, the adhered cells were mostly round in shape, without spreading at 6 h, and some of the cells started to spread after 18 h. However, on the CNT-Chi hybrid coatings (CNT1 to CNT4), many cells already started to spread out as early as 6 h, and at 18 h, most of the cells were highly elongated. Among the CNT-Chi hybrid coating samples, no apparent difference was noted.

The confocal images of cells initially adhered and spread onto the nanostructured hybrid coating substrates were subsequently quantified, in terms of the rates of cytoskeletal extensions (Figure 7b). The fraction of spread cells was significantly higher on the CNT-Chi hybrid coatings, when compared to pure Chi coating (CNT0), at both 6 and 18 h. Only a small fraction of cells were spread on CNT0 at 6 h (~15%), which became ~55% at 18 h. However, on the hybrid coatings, the spread cell fraction was as high as 50−60% at 6 h, and reached over 70% after 18 h. The extension length was also quantified. The average length of the cytoskeletal extensions was significantly higher on the hybrid coatings, than on the pure Chi coating. The results clearly demonstrated the CNT-Chi hybrid coatings enabled the stimulation of osteoblastic cell adhesion processes, including cell anchorage and spreading. The highly elongated morphology of cells on the CNT-Chi hybrid coatings is considered to reflect the underlying nanofibrous-structured topology. In other words, the CNT-aided nanostructured surface should play a key role in the cellular anchorage, and subsequent cytoskeletal extension processes. It has also been accepted that topography, particularly nanotopology, strongly influences the morphology and orientation of living cells, through a phenomenon known as contact guidance, and through integrin-mediated intracellular tension, which would play an essential role in determining the characteristic functions of complex tissues.[43−45]

Next, the adhesive proteins possibly involved in the initial adhesion events of osteoblastic cells were examined. Cells cultured on the coatings were immunostained against adhesive proteins, including *p*-FAK, *p*-paxillin, and vinculin (Figure 8). While the cells cultured on hybrid coatings exhibited stronger signals positive for all the adhesive molecules, those on CNT0 showed very limited signals. Therefore, based on the cell morphological and biochemical results, the importance of the adhesive protein molecules in the initial phase of cellular adhesion and spreading processes is demonstrated. Moreover, the CNT-aided nanostructured surface should function in up-regulation of those adhesive protein complexes.

Ongoing from this adhesion stimulation, the differentiation into osteogenic processes, and much later cellular responses, will be an important and interesting study remaining in the future, to elucidate the potential of the CNT-Chi nanostructured coating substrate for bone repair purposes.

3.5. Protein Loading and Delivery Potential of Hybrid Coatings. As an additional biological performance of the nanostructured hybrid coatings, here we studied the protein loading and delivery capacity. As the model protein, BSA was chosen, and the loading and release behaviors were examined. It is considered that the BSA may be adsorbed mainly by weak electrostatic attractions between negatively charged BSA, and positively charged Chi-CNT surface. Furthermore, the ultra-high surface area enabled by the nanostructured networks is believed to provide effective space and site for the protein incorporation. The nanotubular network structures generated primarily from CNTs will be beneficial for taking up protein molecules at large quantities while the positively charged Chi can play a decisive role in attracting negatively charged molecules like BSA. The BSA adsorption isotherm was first examined with respect to the initial concentration of BSA solution (Figure 9). The loaded amount of BSA onto the coatings increased gradually, with increasing solution concentration. It was obvious that the hybrid coatings showed significantly different BSA loading amount, from the pure Chi coating. Furthermore, the loading amount increased as the CNT content in the coating increased. The maximum loading amount of BSA onto each coating, recorded at 5 mg/mL of initial BSA concentration, was 22 μg for CNT0, 123 μg for CNT1, 157 μg for CNT2, 191 μg for CNT3, and 209 μg for CNT4. The differences between pure Chi (CNT0) and hybrids

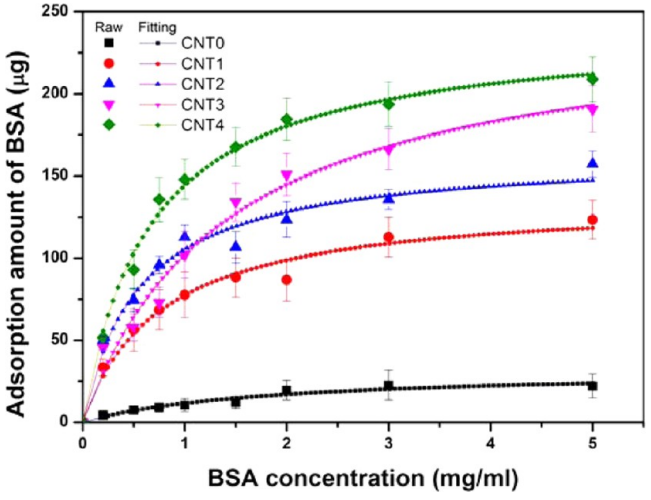

Figure 9. Loading study of protein BSA onto the nanostructured hybrid coatings. BSA loading was monitored with respect to the BSA concentration used initially. Curve fittings were referenced to the modified Langmuir isotherm equation.

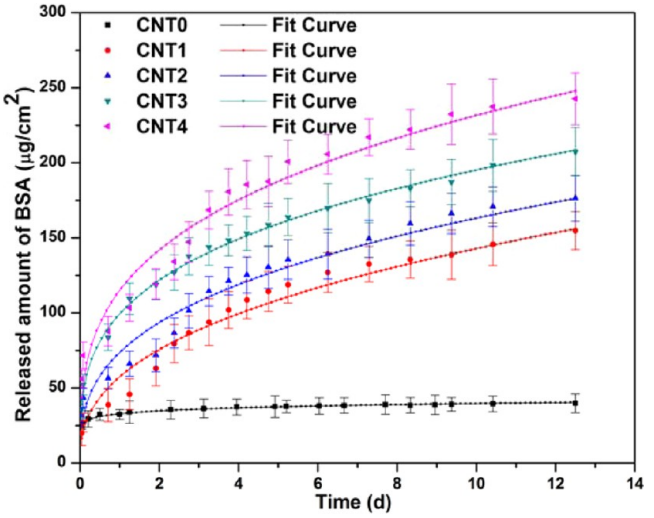

Figure 10. Cumulative release profile of loaded BSA from the coatings, monitored as a function of time. Curve fittings were referenced to the Ritger-Peppas model.

Table 1. Summary of Release-Model Parameters (K and n) of the Coatings Fitted Based on the Ritger-Peppas Empirical Equation ($M_t/M_\infty = Kt^n$)

	specimens				
parameters	CNT0	CNT1	CNT2	CNT3	CNT4
K	25.31	14.36	25.48	18.62	23.23
n	0.084	0.39	0.33	0.42	0.42

were as high as 6−9 times. Because the outermost surface charge characteristic of the hybrid coatings is similar to that of pure Chi coating, due to the Chi decoration of CNTs, such a big difference between the groups is mainly due to the difference in surface area associated with the nanostructured morphology.[46,47] As the Chi-decorated surface is also highly positively charged, the protein charge characteristics should be important, to allow for the charge−charge interactions. In fact, when we tested a positively charged protein (cytochrome C) to load onto the Chi or CNT-Chi coatings, a very minimal amount of protein could be loaded. As soon as the charge property is satisfied, the pore size of the networks and the surface area should determine the protein loading quantity, providing a space for protein penetration, and sites for adsorption. Based on the protein loading result, the positively charged nanostructured CNT-Chi coating was highly effective in taking up biological molecules, which are principally negatively charged.

We next investigated the protein release behaviors from the coatings. The BSA-loaded coatings were soaked in PBS solution at 37 °C, for different time periods, of up to 14 days (Figure 10). From the pure Chi coating (CNT0), the protein release occurred abruptly, showing a burst release within a few hours. Furthermore, 50% was released for the first 1 day, and almost 100% was released in the next 5 days. However, from the hybrid coatings, the BSA release was highly sustainable: BSA continued to release even after 12 days, with curved patterns. In order to delineate the protein release mechanism from the coatings, we fitted the results according to the Ritger-Peppas empirical equation ($M_t/M_\infty = Kt^n$), where the n value is an exponent characterizing the release mechanism. Each parameter determined from the release profile is summarized in Table 1. In the case of CNT0, the n value was 0.084, which means the release behavior of BSA is time independent; rather, the very initial stage (within a few hour) of the release was reasoned to be reaction-controlled. On the other hand, in the case of CNT-Chi hybrid coatings, the n values were around 0.4, which suggests the stage is a sort of anomalous diffusion-controlled (a slight deviation from the Fickian diffusion-controlled) release phenomenon, as has been reported elsewhere.[48,49] Since the bond between BSA and Chi is a kind of weak charge−charge interaction, it easily breaks, due to the ionic exchanges in the saline solution. In the case of CNT0, the BSA molecules could be liberated, as soon as the ionic exchange occurred. However, in the case of CNT-Chi hybrids, the liberated BSA molecules should be released, out through the nanoporous networks of the coatings. The diffusion-controlled release behaviors of BSA from the CNT-Chi hybrid coatings also support this hypothesis. In fact, some other coating methods of preparing nanostructures on Ti have also been carried out to effectively load and deliver protein molecules, which include nanoporous titania coatings and nanocrystalline calcium phosphate coatings.[50−52] For the case of nanoporous titania, the protein loading was not easily implemented although small drug molecules were possibly loaded. Furthermore, the calcium phosphate coatings were shown to release protein molecules only within 10 days while the protein loading capacity could be improved. Therefore, the current CNT-Chi coatings can be considered to have excellent performance in effective loading and sustainable delivery of large molecules like proteins.

Taken from the results on the capacity of the CNT-Chi coatings related to proteins, i.e., high loading capacity of proteins, and their sustained release, the nanostructured hybrid coatings may find additional potential applications in the delivery of protein molecules that are therapeutically relevant for bone repair and regeneration. Further study thus remains as to this therapeutic application of the developed coatings. This prospect, together with the physical merit of the nano-topological feature of the coatings, will contribute to stimulating cellular events, including osteogenic processes; and ultimately, to improving the bone repair ability of coating implants.

4. CONCLUSIONS

Hybrids of Chi and surface-modified CNTs were interfaced onto Ti by the EPD process, with varying compositions. The hybrid coatings were made of Chi-decorated CNTs, featuring nanofibrous structures. The nanostructured hybrid coatings significantly stimulated the initial cell adhesion events, including cell anchorage and spreading, and the expression of adhesive molecules. The hybrid coatings were highly effective for loading of a large quantity of proteins, and releasing them in a sustained manner, over a few weeks, which was enabled by the nanotopographical feature of the coatings. These results suggest that the EPD-enabled nanostructured CNT-Chi hybrid coatings may be potentially useful as the cell-stimulating and therapeutic interfaces of metallic implants, for bone repair and regeneration.

■ ASSOCIATED CONTENT

Supporting Information

Table S1: Designations of the CNT-Chi hybrid coatings and the material concentrations used for the coatings. This material is available free of charge via the Internet at http://pubs.acs.org.

■ AUTHOR INFORMATION

Corresponding Author

*E-mail: kimhw@dku.edu. Tel: +82 41 550 3081. Fax: +82 41 550 3085.

Notes

The authors declare no competing financial interest.

■ ACKNOWLEDGMENTS

This study was supported by grants from the Priority Research Centers Program (2009-0093829), National Research Foundation, South Korea.

■ REFERENCES

(1) Liu, X.; Chu, K. P.; Ding, C. Surface Modification of Titanium, Titanium Alloys, and Related Materials for Biomedical applications. *Mater. Sci. Eng. R* **2004**, *47*, 49−121.

(2) Kim, H. W.; Koh, Y. H.; Li, L. H.; Lee, S.; Kim, H. E. Hydroxyapatite Coating on Titanium Substrate with Titania Buffer Layer Processed by sol−gel Method. *Biomaterials* **2004**, *25*, 2533−2538.

(3) Pilliar, R. M. Modern Metal Processing for Improved Load-Bearing Surgical Implants. *Biomaterials* **1991**, *12*, 95−100.

(4) Dalby, M. J.; Gadegaard, N.; Oreffo, R. O. C. Harnessing Nanotopography and Integrin−Matrix Interactions to Influence Stem Cell Fate. *Nat. Mater.* **2014**, *13*, 558−569.

(5) Skorb, E. V.; Andreeva, D. V. Surface Nanoarchitecture for Bio-Applications: Self-Regulating Intelligent Interfaces. *Adv. Funct. Mater.* **2013**, *23*, 4483−4506.

(6) Yim, E. K.; Darling, E. M.; Kulangara, K.; Guilak, F.; Leong, K. W. Nanotopography-Induced Changes in Focal Adhesions, Cytoskeletal Organization, and Mechanical Properties of Human Mesenchymal Stem Cells. *Biomaterials* **2010**, *31*, 1299−1306.

(7) Perez, R. A.; Won, J. E.; Knowles, J. C.; Kim, H. W. Naturally and Synthetic Smart Composite Biomaterials for Tissue Regeneration. *Adv. Drug. Delivery Rev.* **2013**, *65*, 471−496.

(8) McNamara, L. E.; Sjostrom, T.; Meek, R. M. D.; Su, B.; Dalby, M. J. Investigation of the Limits of Nanoscale Filopodial Interactions. *J. Tissue Eng.* **2014**, *5*, 2041731414536177.

(9) Kurzweg, H.; Heimann, R. B.; Troczynski, T. Development of Plasma Sprayed Bioceramic Coatings with Bond Coats Based on Titania and Zirconia. *Biomaterials* **1998**, *19*, 1507−1515.

(10) Jun, S. H.; Lee, E. J.; Yook, S. W.; Kim, H. E.; Kim, H. W. A Bioactive Coating of a Silica Xerogel−Chitosan Hybrid on Titanium by a Room Temperature sol−gel Process. *Acta Biomater.* **2010**, *6*, 302−307.

(11) Barrere, F.; Blitterswijk, C. A. V.; Groot, K. D.; Layrolle, P. Nucleation of Biomimetic Ca-P Coating on Ti6Al4V from a SBF X 5 Solution: Influence of Magnesium. *Biomaterials* **2002**, *23*, 2211−2220.

(12) Li, L. H.; Kong, Y. M.; Kim, H. W.; Kim, Y. W.; Kim, H. E.; Heo, S. J.; Koak, J. Y. Improved Biological Performance of Ti Implants Due to Surface Modification by Micro-Arc Oxidation. *Biomaterials* **2004**, *25*, 2867−2875.

(13) Kim, K. H.; Ramaswamy, N. Electrochemical Surface Modification of Titanium in Dentistry. *Dent. Mater. J.* **2009**, *28*, 20−36.

(14) Zhitomirsky, I.; Gol-Or, L. Electrophoretic Deposition of Hydroxyapatite. *J. Mater. Sci.: Mater. Med.* **1997**, *8*, 213−219.

(15) Boccaccini, A. R.; Roether, J. A.; Thomas, B. J. C.; Shaffer, M. S. P.; Chavez, E.; Stoll, E.; Minay, E. J. The Electrophoretic Deposition of Inorganic Nanoscale Materials. *J. Ceram. Soc. Jpn.* **2006**, *114*, 1−14.

(16) Corni, I.; Ryan, M. P.; Boccaccini, A. R. Electrophoretic Deposition: From Traditional Ceramics to Nanotechnology. *J. Eur. Cer. Soc.* **2008**, *28*, 1353−1367.

(17) Simchi, A.; Pishbin, F.; Boccaccini, A. R. Electrophoretic Deposition of Chitosan. *Mater. Lett.* **2009**, *63*, 2253−2255.

(18) Patel, K. D.; Singh, R. K.; Lee, E. J.; Han, C. M.; Won, J. E.; Knowles, J. C.; Kim, H. W. Tailoring Solubility and Drug Release from Electrophoretic Deposition Chitosan-Gelatin Film on Titanium. *Surf. Coat. Technol.* **2014**, *242*, 232−236.

(19) Patel, K. D.; Fiqi, A. E.; Lee, H. Y.; Singh, R. K.; Kim, D. A.; Lee, H. H.; Kim, H. W. Chitosan-Nanobioactive Glass Electrophoretic Coatings with Bone Regenerative and Drug Delivering Potential. *J. Mater. Chem.* **2012**, *22*, 24945−24956.

(20) Pishbin, F.; Mourino, V.; Flor, S.; Kreppel, S.; Salih, V.; Ryan, M. P.; Boccaccini, A. R. Electrophoretic Deposition of Gentamicin-Loaded Bioactive Glass/Chitosan Composite Coatings for Orthopaedic Implants. *ACS Appl. Mater. Interfaces* **2014**, *6*, 8796−8806.

(21) Zhu, M.; Zhu, Y.; Ni, B.; Xie, N.; Lu, X.; Shi, J.; Zeng, Y.; Guo, X. Mesoporous Silica Nanoparticles/Hydroxyapatite Composite Coated Implants to Locally Inhibit Osteoclastic Activity. *ACS Appl. Mater. Interfaces* **2014**, *6*, 5456−5466.

(22) Thomas, B. J. C.; Bocaccini, A. R.; Shaffer, M. S. P. Multi-walled carbon nanotube coatings using electrophoretic deposition (EPD). *J. Am. Ceram. Soc.* **2005**, *88*, 980−982.

(23) Lu, Y.; Li, Tao.; Zhao, X.; Li, M.; Cao, Y.; Yang, H.; Duan, Y. Y. Electrodeposited Polypyrrole/Carbon Nanotubes Composite Films Electrodes for Neural Interfaces. *Biomaterials* **2010**, *31*, 5169−5181.

(24) Qin, N. C.; Zhao, X.; Hirahara, K.; Miyamoto, Y.; Iijima, S. Materials Science: The Smallest Carbon Nanotube. *Nature* **2000**, *408*, 50.

(25) Karousis, N.; Tangmatarchis, N. Current Progress on the Chemical Modification of Carbon Nanotubes. *Chem. Rev.* **2010**, *110*, 5366−5397.

(26) Zheng, M.; Jagota, A.; Semke, E. D.; Diner, B. A.; Mclean, R. S.; Lusting, S. R.; Richardson, R. E.; Tass, N. G. DNA-Assisted Dispersion and Separation of Carbon Nanotubes. *Nat. Mater.* **2003**, *2*, 338−342.

(27) Iijima, S. Helical Microtubules of Graphitic Carbon. *Nature* **1991**, *354*, 56−58.

(28) Allaoui, A.; Bai, S.; Cheng, H. m.; Bai, J. B. Mechanical and Electrical Properties of a MWNT/Epoxy Composite. *Compos. Sci. Technol.* **2002**, *62*, 1993−1998.

(29) Illum, L. Chitosan and Its Use as a Pharmaceutical Excipient. *Pharm. Res.* **1998**, *15*, 1326−1331.

(30) Rinaudo, M. Chitin and Chitosan: Properties and Applications. *Prog. Polym. Sci.* **2006**, *31*, 603−632.

(31) Hwang, J. Y.; Shin, U. S.; Jang, W. C.; Hyun, J. K.; Wall, I. B.; Kim, H. W. Biofunctionalized Carbon Nanotubes in Neural Regeneration: A mini Review. *Nanoscale* **2013**, *5*, 487−497.

(32) Singh, R. K.; Patel, K. D.; Kim, J. J.; Kim, T. H.; Kim, J. H.; Shin, U. S.; Lee, E. J.; Knowles, J. C.; Kim, H. W. Multifunctional Hybrid Nanocarrier: Magnetic CNTs Ensheathed with Mesoporous Silica for

Drug Delivery and Imaging System. *ACS Appl. Mater. Interfaces* **2014**, *6*, 2201−2208.
(33) Sarkar, P.; Nicholson, P. S. Electrophoretic Deposition (EPD): Mechanism, Kinetics and Application to Ceramics. *J. Am. Ceram. Soc.* **1996**, *79*, 1987−2002.
(34) Liu, L.; Qin, Y.; Guo, Z. X.; Zhu, D. Reduction of Solubilized Multi-Walled Carbon Nanotubes. *Carbon* **2003**, *41*, 331−335.
(35) Bahr, J. L.; Yang, J.; Kosynkin, D. V.; Bronikowski, M. J.; Smalley, R. E.; Tour, J. M. Functionalization of Carbon Nanotubes by Electrochemical Reduction of Aryl Diazonium Aalts: A Bucky Paper Electrode. *J. Am. Chem. Soc.* **2001**, *123*, 6536−6542.
(36) Reddy, K. R.; Sin, B. C.; Ryu, K. S.; Kim, J. C.; Chung, H.; Lee, Y. Conducting Polymer Functionalized Multi-Walled Carbon Nanotubes with Noble Metal Nanoparticles: Synthesis, Morphological Characteristics and Electrical Properties. *Synth. Met.* **2009**, *159*, 595−603.
(37) Zhu, J.; Peng, H.; Rodriguez, M. F.; Margrave, J. L.; Khabashesku, V. N.; Imam, A. M.; Lozano, K.; Barrera, E. V. Reinforcing Epoxy Polymer Composites Through Covalent Integration of Functionalized Nanotubes. *Adv. Funct. Mater.* **2004**, *14*, 634−648.
(38) Yan, L. Y.; Poon, Y. F.; Park, M. B. C.; Chen, Y.; Zhang, Q. Individually Dispersing Single-Walled Carbon Nanotubes with Novel Neutral pH Water-Soluble Chitosan Derivatives. *J. Phys. Chem. C* **2008**, *112*, 7579−7587.
(39) Pranato, Y.; Rakshit, S. K.; Salokhe, V. M. Enhancing Antimicrobial Activity of Chitosan Film by Incorporating Garlic Oil, Potassium Sorbate and Nisin. *LWT-Food Sci. Technol.* **2005**, *38*, 859−865.
(40) Hartgerink, J. D.; Beniash, E.; Stupp, S. I. Self-Assembly and Mineralization of Peptide-Amphiphile Nanofibers. *Science* **2001**, *294*, 1684−1688.
(41) Wei, G.; Reichert, J.; Bossert, J.; Jandt, K. D. Novel Biopolymeric Template for the Nucleation and Growth of Hydroxyapatite Crystals Based on Self-Assembled Fibrinogen Fibrils. *Biomacromolecules* **2008**, *9*, 3258−3267.
(42) He, G.; Ramachandran, A.; Dahl, T.; George, S.; Schultz, D.; Cookson, D.; Veis, A.; George, A. Phosphorylation of Phosphophoryn is Crucial for Its Function as a Mediator of Biomineralization. *J. Biol. Chem.* **2005**, *280*, 33109−33114.
(43) Mendonca, G.; Mendonca, D. B. S.; Aragao, F. J. L.; Cooper, L. F. Advancing Dental Implant Surface Technology- From Micron to Nanotopography. *Biomaterials* **2008**, *29*, 3822−3835.
(44) Lord, M. S.; Foss, M.; Besenbacher, F. Influence of Nanoscale Surface Topography on Protein Adsorption and Cellular Response. *Nano Today* **2010**, *5*, 66−78.
(45) Wang, Y. J.; Lo, T. Y.; Wu, C. H.; Liu, D. M. Electrophoretic Coating of Amphiphilic Chitosan Colloids on Regulating Cellular Behaviour. *J. R. Soc. Interface* **2013**, *10*, 20130411.
(46) Roach, P.; Farrar, D.; Perry, C. C. Surface Tailoring for Controlled Protein Adsorption: Effect of Topography at the Nanometer Scale and Chemistry. *J. Am. Chem. Soc.* **2006**, *128*, 3939−3945.
(47) Srivashtava, S.; Verma, A.; Frankamp, B. L.; Rotello, V. M. Controlled Assembly of Protein Nanoparticle Composites through Protein Surface Recognition. *Adv. Mater.* **2005**, *17*, 617−621.
(48) Ritger, P. L.; Peppas, N. A. A Simple Equation for Description of Solute Release II. Fickian and Anomalous Release from Swellable Devices. *J. Controlled Release* **1987**, *5*, 37−42.
(49) Koutsopoulos, S.; Unsworth, L. D.; Nagai, Y.; Zhang, S. Controlled Release of Functional Proteins Through Designer Self-Assembling Peptide Nanofibers Hydrogel Scaffold. *Proc. Natl. Acad. Sci. U.S.A.* **2009**, *106*, 4623−4628.
(50) Ketabchi, A.; Komm, K.; Rossouw, M. M.; Cassani, D. A. D.; Variola, F. Nanoporous Titanium Surfaces for Sustained Elution of Proteins and Antibiotics. *PloS One* **2014**, *9*, 1−9.
(51) Yu, X.; Wei, M. Controlling Bovine Serum Albumin Release from Biomimetic Calcium Phosphate Coatings. *J. Biomater. Nanobiotechnol.* **2011**, *2*, 28−35.
(52) Wen, H. B.; Wijn, J. R. de.; Blitterswijk, C. A. van.; Groot, K. de. Incorporation of Bovine Serum Albumin in Calcium Phosphate Coating on Titanium. *J. Biomed. Mater. Res. Part A* **1999**, *46*, 245−252.